A Monte Carlo Analysis of Error Associated With Two-Wavelength Algorithms for Retinal Oximetry

Daniel A. Rodriguez,[1] T. Joshua Pfefer,[2] Quanzeng Wang,[2] Pedro F. Lopez,[3] and Jessica C. Ramella-Roman[1,3]

[1]Department of Biomedical Engineering, Florida International University, Miami, Florida, United States
[2]Food and Drug Administration, Center for Devices and Radiological Health, Silver Spring, Maryland, United States
[3]Herbert Wertheim College of Medicine, Florida International University, Miami, Florida, United States

Correspondence: Jessica C. Ramella-Roman, Department of Biomedical Engineering, Florida International University, 10555 W. Flagler Street, EC-2610, Miami, FL 33174, USA; jramella@fiu.edu.

Submitted: June 16, 2016
Accepted: October 23, 2016

Citation: Rodriguez DA, Pfefer TJ, Wang Q, Lopez PF, Ramella-Roman JC. A Monte Carlo analysis of error associated with two-wavelength algorithms for retinal oximetry. *Invest Ophthalmol Vis Sci*. 2016;57:6474–6481. DOI:10.1167/iovs.16-20138

Purpose. Two-wavelength algorithms aimed at the extrapolation of retinal vasculature optical properties are being used in the clinical setting. Although robust, this approach has some clear mathematical limitations. We have conducted an in-depth study of this methodology and report on the limits and benefit of this approach.

Methods. We used a well-tested, voxel-based Monte Carlo model of light transfer into biological tissue combined with a seven-layer model of the human fundus to create reflectance maps of retina vessels at different oxygenation levels.

Results. This study shows that the two-wavelength approach works remarkably well in the optimal scenario of known calibration arteries and veins. Errors as a result of choroidal pigmentation and discrepancies in vessel size can be minimized with numerical approaches. When the calibration process deviates largely from physiological values, the technique fails with large errors.

Conclusions. The two-wavelength approach is convenient, easy to implement, and suitable in studies where relative rather than absolute knowledge of retinal oximetry is necessary. A robust calibration step is paramount when using this approach.

Keywords: oximetry, two-wavelength, Monte Carlo

Accurate and reliable measurements of retinal vasculature hemoglobin oxygen saturation (SO_2) can provide key insight into the pathophysiological status of the eye. Unusual saturation levels have been linked to different ocular diseases, including diabetic retinopathy, retinopathy of prematurity, photoreceptor degeneration, and visual loss.[1–3] The course of treatment is often contingent on the stage of the disease.[4,5]

Recently retinal oximeters have been tested on healthy individuals[6–10] and used to investigate diabetic retinopathy,[11,12] glaucoma,[13–17] ocular hypertension,[13] Eisenmenger syndrome,[18] macular degeneration,[19] retinitis pigmentosa,[20] vein occlusions,[21–23] and artery occlusions.[24] Several authors are reporting high reproducibility in their oximetry measurements,[10,25,26] yet most researchers agree that measurement values obtained with retinal oximetry must be considered as relative values and not absolute. As this technology enters the clinical realm it is paramount to accurately measure its strength and limitation.

Over the years many groups have turned to spectroscopic techniques to measure retinal SO_2. An excellent review of these techniques is available here.[27] To summarize briefly, Hickam et al.[28] used a two-wavelength apparatus to measure retinal vein oxygen saturation in 1963. Two-wavelength systems exploit hemoglobin's absorbance spectrum at one isosbestic point and at a wavelength different from the isosbestic point.[29,30] Three-wavelength retinal oximeters were also proposed,[31,32] taking into account the scattering of red blood cells in blood.[33] Multispectral techniques were also utilized by several groups both with point measurements and imaging.[34–36]

In recent years, however, there has been a revival of the two-wavelength retinal oximetry approach.[37–39] These systems are generally developed utilizing a fundus camera combined with a scientific grade digital camera. The light illuminating the retina is either filtered before impinging on the eye or at the detector. Typical wavelengths combinations are 586/605 nm,[40] 570/600 nm,[7] and 548/610 nm.[39]

It has been shown that the accuracy of retinal oximeters is affected by factors such as variations in vessel size,[39,41–43] changes in total or heterogeneous distribution of pigmentation in the eye,[39,42] and crosstalk with hemoglobin in the choroidal vasculature.[42,44] Algorithms compensating for these factors have been proposed.[29,39]

In this study, we utilize a well-calibrated, voxel-based Monte Carlo[45,46] model of light transport to analyze the error associated with two-wavelength algorithms under different scenarios. We investigate the accuracy of these algorithms for incorrect assumption of SO_2 in the calibration step, for variations of vessel diameter, for variations in choroidal pigmentation, and for choroidal vessel crosstalk.

The two-wavelength algorithm as originally reported by Beach et al.[29] and later by Hardarson et al.[40] is based on the calculation of the optical density (OD) of the retina at two different wavelengths. By measuring the reflectance on the vessel (I) and next to the vessel (I_0), the OD at each wavelength is calculated using Equation 1.

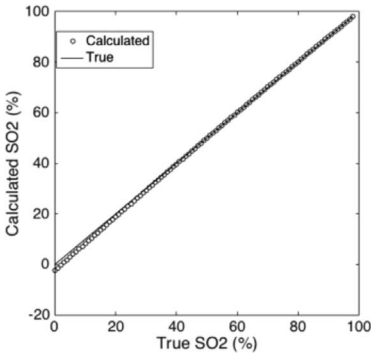

Figure 1. Mathematical calculation of SO_2 of whole blood using two-wavelength algorithms in a simplified 100-μm vessel with perfect calibration assumptions.

$$OD_\lambda = \log(I_0/I) \quad (1)$$

The OD ratio (ODR) is defined as the ratio of the ODs at two different wavelengths (Equation 2).

$$ODR = OD_{\lambda_1}/OD_{\lambda_2} \quad (2)$$

OD_{λ_1} is the OD at one wavelength (λ_1) andOD_{λ_2} is the OD at a different wavelength. ODR is assumed to have a linear relationship with SO_2, hence Equation 3 is used to calculate the oxygen saturation within a vessel,

$$SO_2 = a + ODR \times k \quad (3)$$

where a and k are constants obtained through a calibration procedure.

Based on SO_2 values for arteries and veins reported by several investigators,[28,32,47,48] we estimate typical values to be 96% and 54%, respectively. The optical density ODR of first-degree arteries and veins are also calculated with the retinal oximeter on healthy individuals. For example, Hardarson reported $ODR_a = 0.209$ for arteries and $ODR_v = 0.502$ on veins based on a study of 18 healthy individuals.

By assuming a linear relationship between ODR and SO_2, a and k can be calculated by solving the equation pair.

$$\begin{aligned} 96\% &= a + k \times ODR_a \\ 54\% &= a + k \times ODR_v \end{aligned} \quad (4)$$

Finally, once a and k are known, Equation 3 can be used to extrapolate any vessel oxygen saturation level.

In this paper, we will explore this straightforward mathematical approach for the quantification of retinal oximetry using a Monte Carlo framework.

Methods

Two-Wavelength SO_2 Algorithm

We start our analysis of the two-wavelength approach by making several simplifications. First, we assume that blood does not contain any scatterer but contains only hemoglobin and that the Beer-Lambert law[49] can be applied to quantify the transmission of light through a sample. Second, we assume that no other absorber is present in the optical path aside from hemoglobin at various levels of oxygenation. Using tabulated data of human oxygenated and deoxygenated hemoglobin,[49] we can then calculate transmittance values through samples of a predetermined size.

A blood sample of 100 μm length is selected first. The oxygen saturation of the blood is set first at 96% and then at 54%, mimicking reported values of retinal arterial and venous oxygenation, respectively. OD values at two wavelengths, 570 and 600 nm, are calculated for the two oxygenation levels. Using Equation 2, their respective ODR is also calculated, and finally a and k are calculated using Equation 4. This step mimics a perfect calibration scenario where all of the elements of the experiment are known.

Then SO_2 levels in the test vessel are allowed to change from 0% to 98% with a 1% step. The vessel SO_2 is obtained using the previous values of a and k and Equation 2. The results of the calculated values are compared with the expected value of SO_2, Figure 1. Even in this oversimplified approach an error is produced, especially toward lower values of SO_2. At physiological relevant levels of SO_2 (40% to 100%), the error is a very low < 0.1 percentage points.

We now investigate the error resulting from faulty calibration assumptions. For this step we still rely on a simplified vessel of 100-μm diameter with no other absorber aside from hemoglobin, and the test vessel is set at 98% SO_2. For calibration, a representative artery and vein are necessary (Equation 4). The representative arterial value from the literature (96%) was used. In this test, the SO_2 of the calibration artery was varied from 90% to 100%. Figure 2b shows how a faulty calibration assumption impacts the calculated results of SO_2 for the test vessel. The further the calibration true value is from the assumption of 96%, the higher is the error. The same process is followed for a faulty assumption of calibration vein SO_2, with the test vessel in this case being a vein at 58% SO_2. The assumed value for calibration is 54% (Equation 2), whereas the true value of the calibration vessel is varied between 40% and 60%.

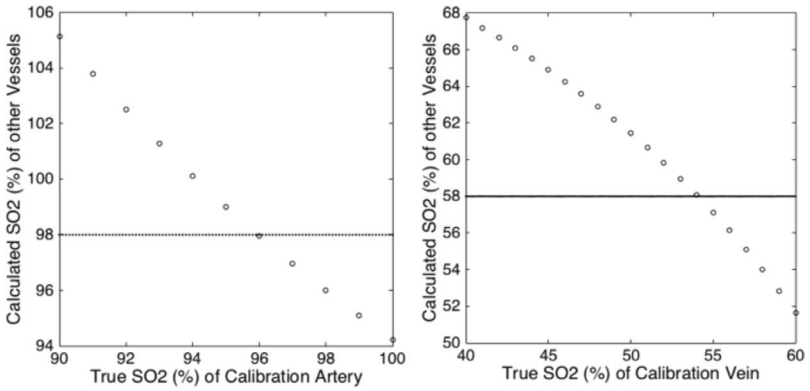

Figure 2. Mathematical calculation of SO_2 of whole blood using two-wavelength algorithms with an (**a**) incorrect calibration artery assumption and (**b**) incorrect calibration vein assumption.

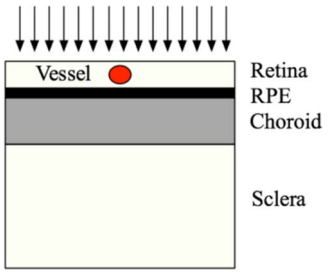

FIGURE 3. Eye model geometry (not to scale).

Figure 2b shows deviation from the expected calculated value of SO2 for a 58% vein as a result of faulty calibration parameters.

In this section, we used a highly simplified scenario to model retinal oximetry. To truly test the efficacy of the two-wavelength algorithm, we need to take into account all of the various absorbers and scatterers of the fundus. Such a study can only be conducted through computational models. Here we use a well-tested Monte Carlo framework to simulate light transport through a realistic eye.

Monte Carlo

Monte Carlo modeling is a well-established method of analyzing light transport through tissue.[50,51] A voxel-based Monte Carlo model was utilized in this work.[45] This model allows for the analysis of three-dimensional geometries with heterogeneous structures. Photons are launched and traced independently, propagating within voxels experiencing scattering and/or absorption events, depending on the optical properties of the tissues being modeled. Each voxel may represent a different tissue or structure based on the optical properties assigned to it. Voxel sizes were 4 μm in length, width, and height. Two hundred million photons were launched in each simulation. Photons reflected out of the geometry were recorded to obtain intensity images of the geometry under investigation. Prior to conducting any test, our model was further validated against a Monte Carlo model of photon transport in multilayered tissue[50] and resulted in errors well below statistical significance.

Eye Model

Our simplified model (Fig. 3) takes into account the main absorbing and scattering layers of the eye, including the neural retina, the retinal pigment epithelium (RPE), the choroid, and the sclera. Other layers in the eye were ignored for our simulations because they have been reported to be optically thin and do not affect photon propagation as much as the main layers represented in the model.[51] Utilizing the advantages of the voxel-based analysis, we embedded a vessel within the retinal layer. Our tissue geometry of investigation spanned a volume of 800 μm by 800 μm laterally with a tissue thickness of 1160 μm, with retinal thickness of 20 0μm, RPE thickness of 10 μm, choroid thickness of 250 μm, and sclera thickness of 700 μm.[52] A vessel was placed 10 μm below the surface of the neural retina. Unless otherwise stated, the calibration vessels were 100 μm in diameter, and the detection vessel diameter was varied in different tests. The optical properties of the layers at the wavelengths of interest can be seen in the Table.

TABLE. Optical Properties

Geometry Layers	Optical Properties	570 nm	600 nm
Retina, 200 μm	μ_a[52]	4.71 cm^{-1}	3.6 cm^{-1}
	μ_s[52]	30.89 cm^{-1}	28.57 cm^{-1}
	g[52]	0.97	0.97
RPE, 10 μm	μ_a[53,54]	208.21 cm^{-1}	174.47 cm^{-1}
	μ_s[52]	1197.91 cm^{-1}	1225.08 cm^{-1}
	g[52]	0.84	0.84
Choroid, 250 μm	μ_a[49]	477.52 cm^{-1}	277.50 cm^{-1}
	μ_s[52]	708.64 cm^{-1}	622.69 cm^{-1}
	g[52]	0.945	0.945
Sclera, 700 μm	μ_a[52]	3.89 cm^{-1}	3.34 cm^{-1}
	μ_s[52]	915.95 cm^{-1}	876.63 cm^{-1}
	g[52]	0.9	0.9

μa, absorption coefficient; μs, scattering coefficient; g, anisotropy.

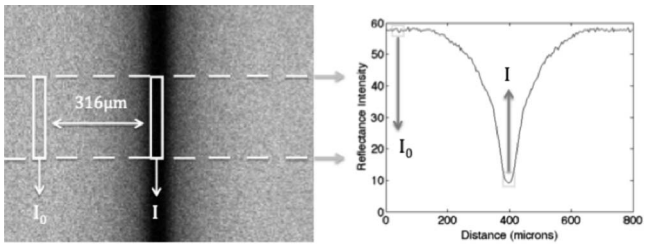

FIGURE 4. (**a**) Simulated fundus reflectance image based on an idealized retinal geometry including layered tissue with an embedded vessel (*top*). Reflection intensities I_0 and I are calculated by averaging intensity values in the background and on the vessel, respectively. (**b**) Average reflection intensity, from (panel **a**). I_0 was calculated far enough from the vessel, where the background intensity was constant and not affected by the absorbance of the vessel. Intensity profile of a 94% SO_2 vessel in the retina, captured at 570 nm.

The absorption coefficient of the RPE has been reported by several sources, yet there does not seem to be a consensus in the value mainly because of disagreements in melanin concentration reports.[52,55,56] Melanin is known to be a strong absorber and has been extensively studied because of its prevalence in the skin and retina. Glickman et al.[53] reported melanin to have an absorption coefficient of 2237 cm^{-1}. Feeney-Burns et al.[54] showed that the RPE can be estimated to be composed of approximately 12% melanin.

The choroid consists of melanin and blood vessels. In our simulation, the absorption coefficient of the choroid was taken as the sum of the absorption coefficient of the blood and melanin in this layer. Blood comprises approximately 70% of the volume of this region and typically has a saturation of 95%. Melanin concentration in the choroid, similar to the RPE, has many different reported values. Because the iris and the choroid are both the same layer in the eye, we used a melanin concentration of 26 mg/cm^3 as reported by Koblova et al.[57] The absorption and scattering coefficients of blood were calculated from data published by Bosschaart et al.[49] The assignment of scattering angles is achieved in the Monte Carlo through a Henyey Greenstein phase function,[58] and this has been shown to provide an effective phase function for blood with physiological haematocrit in the visible range.[59] The index of refraction for all layers was kept at 1.37.

As shown in Figure 4a, a region of interest within the reflected image was selected, and pixels within that region were averaged. The width of the region of interest was 25% of the corresponding vessel diameter and a fixed length of 720 μm. I_0 was calculated by averaging reflection intensities within a neighboring area of the vessel. To be certain that I_0 was not affected by the vessel (Fig. 4b), I_0 was calculated $>$ 316 μm away from I (Fig. 4a). I was calculated by averaging reflection intensities within 25% of the corresponding vessel diameter around the center of the vessel.

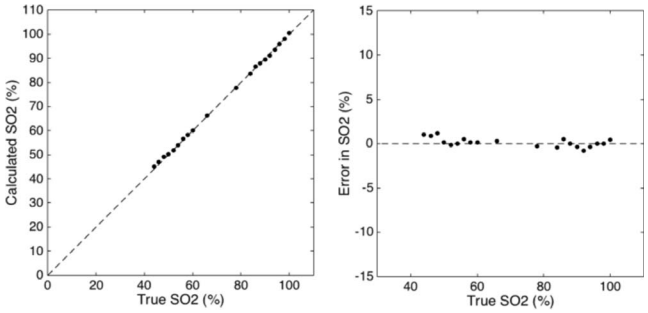

FIGURE 5. Two-wavelength oximetry using 570 and 600 nm. (**a**) Calculated SO_2 measurements on different vessels whose actual SO_2 ranged from 44% to 100%. Calculations were performed under a correctly calibrated algorithm where the calibration vessel SO_2 assumptions were correct. (**b**) Error in calculated SO_2 for each vessel.

In this paper, the calibration was performed by creating reflection images of a perfect artery ($SO_2 = 96\%$) and a perfect vein ($SO_2 = 54\%$). ODR for each vessel was then computed, and their actual SO_2 was used within the algorithm. Under this assumption, constants a and k were calculated by solving a simple system of equations.

RESULTS

Utilizing the Monte Carlo approach, various experimental scenarios were implemented to characterize the effect of calibration assumptions on SO_2 measurement accuracy.

Choice of Wavelength Pair

Figures 5a and 5b show the case where the calibration assumptions were correct. In this test, 570 and 600 nm wavelengths were utilized. Vessels with SO_2 levels ranging from 44% to 100% were included in the geometry of Figure 3.

Some investigators have devised systems[60] using 520 and 630 nm as the primary wavelengths. This strategy is necessary because of the particular experimental layout (single camera) as well as the necessity of simultaneously measuring oxygenation and flow. Here we show the impact of the choice of different wavelength pairs in the accuracy of the two-wavelength algorithm. In this scenario, calibration was performed using vessels of 100 μm in diameter and assumed SO_2 of 54% and 96% for the calibration vein and artery, respectively. Figures 6a and 6b show the ideal case where the calibration assumptions were correct. Results were similar to those produced using 570 and 600 nm wavelengths, although a higher error is shown at very low SO_2 levels ($SO_2 < 45\%$).

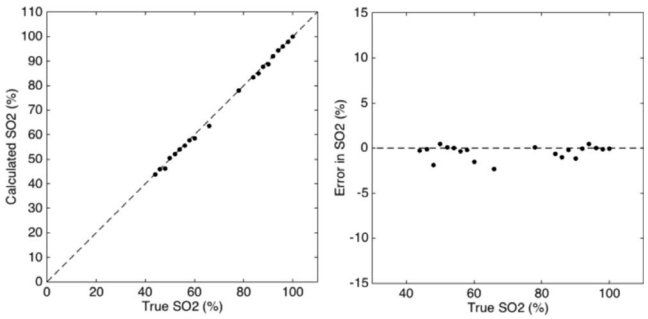

FIGURE 6. Two-wavelength oximetry using 520 and 630 nm. (**a**) Calculated SO_2 measurements on different vessels whose actual SO_2 ranged from 44% to 100%. Calculations were based on a correctly calibrated algorithm where the calibration vessel SO_2 assumptions were correct. (**b**) Error in calculated SO_2 for each vessel.

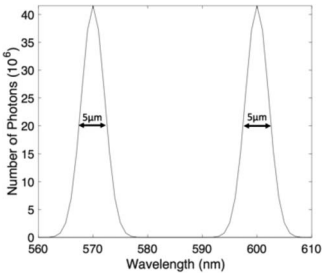

FIGURE 7. Number of photons launched per wavelength for two filters with a full width half max of 5 nm and centered at 570 and 600 nm, respectively, totaling 200,000,000 photons.

Filter Bandwidth

Dual-wavelength retinal oximeters capture two fundus images of the same area of the retina. In this section, we study the effect of illumination and detection filter bandwidth on SO_2 measurement accuracy. A 570 and 600 nm wavelength pair was used with 5-nm band-pass filters centered at these wavelengths. The choice of wavelength and filter bandwidth is guided by current methodologies.[7] Implementing a 5-nm band-pass filter was achieved by assuming a Gaussian distribution centered at each wavelength with a full width half max of 5 nm to calculate the amount of photons launched per wavelength, as shown in Figure 7.

Simulations were run for wavelengths 567 to 573 nm and 597 to 603 nm, with a step size of 1 nm. Reflection intensity profiles were obtained for each wavelength and summed for each group. The summed reflection intensities centered at 570 and 600 nm were generated for vessels with SO_2 ranging from 44% to 100%. The equations were calibrated based on correct assumptions of SO_2. The results are shown in Figures 8a and 8b.

Incorrect Calibration Assumption. In the introductory section of this paper, we described current methods for device calibration. This is performed by assigning SO_2 values to an artery and vein relating as a way to establish a linear relationship between ODR and SO_2. The assumed values are based on previous work by different investigators. In the ideal case we have shown how this approach introduces an inherent error whose magnitude depends on the degree of separation between assumed and true calibration values. Utilizing this model, we tested cases where the assumed SO_2 values used for the calibration vein and artery (54% and 96%) were incorrect.

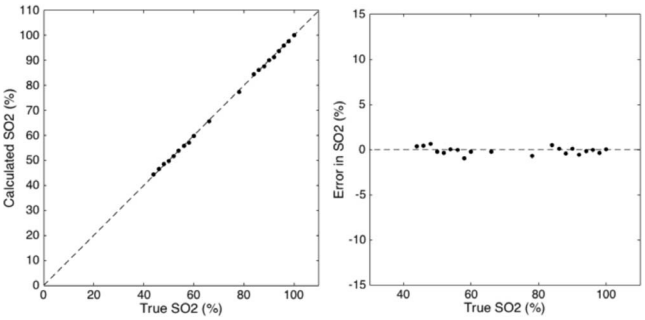

FIGURE 8. (**a**) Calculated SO_2 measurements for vessels whose actual SO_2 ranged from 44% to 100%. Calculations were performed under a correctly calibrated algorithm where the calibration vessel SO_2 assumptions were correct. (**b**) Error in calculated SO_2 for each vessel.

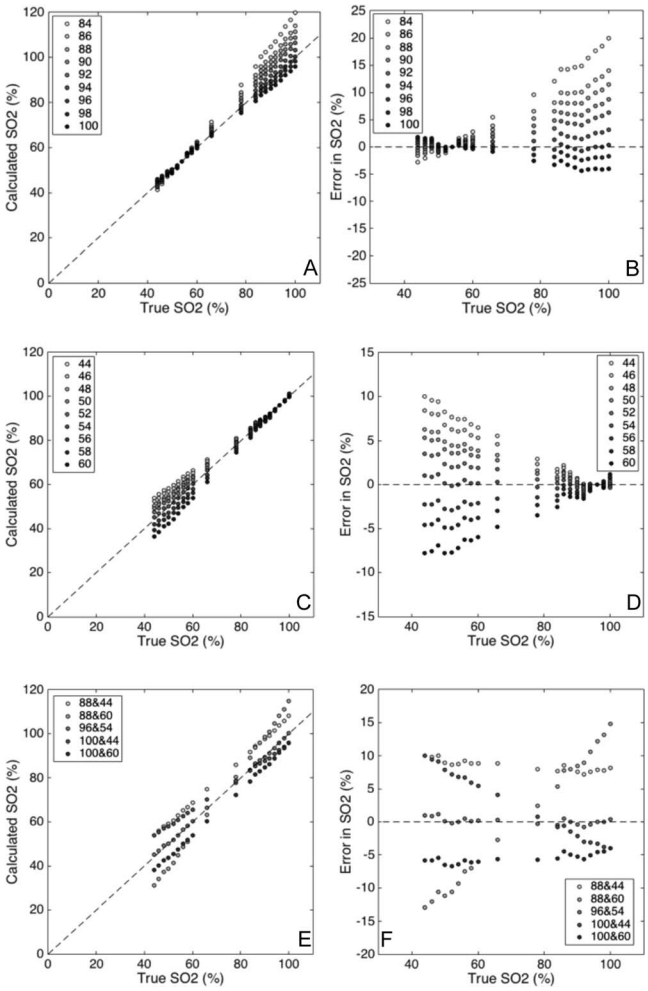

Figure 9. (**a**) Data on measured SO_2 when the assumed SO_2 (54%) of the calibration vein was correct but the assumed SO_2 (96%) of the calibration artery was incorrect, where the actual calibration artery SO_2 ranged from 84% SO_2 to 100% SO_2. (**b**) The error of measured SO_2 for vessels measured with this incorrectly calibrated algorithm as a result of the incorrect assumed SO_2 of the calibration artery. (**c**) Data when the assumed SO_2 of the calibration artery was correct but the assumed SO_2 of the calibration vein was incorrect, where the actual SO_2 ranged from 44% to 60% SO_2. (**d**) The error in measured SO_2 for vessels measured with this incorrectly calibrated algorithm as a result of the incorrect assumed SO_2 of the calibration vein. (**e**) Data of measured SO_2 when the assumed calibration artery and vein SO_2 were incorrect, with different actual SO_2s presented in the legend. (**f**) The error in measured SO_2 for vessels measured with this incorrectly calibrated algorithm as a result of the incorrect assumed SO_2 of the calibration vein and artery.

SO_2 calculations were performed on fundus vasculature with varying oxygen saturations: 44% to 100% SO_2 in steps of 2%.

As seen in Figures 9a and 9b, vessels measured with a device employing an incorrect calibration artery SO_2 assumption can produce widely varying levels of error. When the calibration artery is assumed to be 96% SO_2 but its true value is 84% SO_2, a vessel with 100% SO_2 will be calculated as having values of up to 20 percentage points greater than its true level. Similar results are presented in Figures 4c and 4d, where the calibration vein SO_2 was assumed incorrectly. The actual SO_2 of calibration veins ranged from 44% to 60%. Errors in SO_2 were up to 10 percentage points. Figures 9e and 9f show the case where SO_2 was assumed incorrectly for both the calibration artery and vein. In these cases, errors in estimating SO_2 approached 15 percentage points.

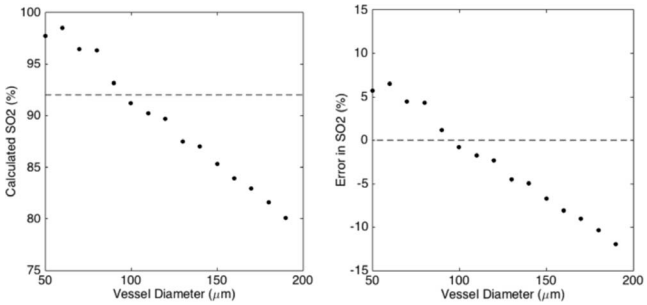

Figure 10. (**a**) Calculated SO_2 under correctly assumed calibration conditions of retinal vessels with diameters ranging from 50 to 190 μm. (**b**) The error of the calculated SO_2.

Vessel Diameter. Vessel diameter has been shown to be an important parameter in the calculation of oxygen saturation. Monte Carlo simulations were performed on vessels with varying diameters. In this scenario, calibration vessel SO_2 values were assumed correctly. SO_2 was measured for blood vessels with SO_2 equal to 92% and diameters ranging from 50 to 190 μm in steps of 10 μm, utilizing a reference vessel of diameter equal to 100 μm. Figure 10a shows the calculated SO_2 for each vessel; these values exhibit a strong monotonic decrease with vessel size. Errors resulting from very large vessels (190 μm in diameter) were as large as 11.9 percentage points below true vessel SO_2 (92%).

Correction for Vessel Diameter

To minimize the error in SO_2 introduced by vessel diameter, Geirsdottir et al.[7] developed a vessel size correction. The correction factor assumes that the SO_2 of a vessel just before a bifurcation is the same as those in both branches after the bifurcation. Equation 5 was used to calculate k, a correction factor, where $SO_{2(\text{uncor},\text{sec}_1)}$, $SO_{2(\text{uncor},\text{sec}_2)}$, and $SO_{2(\text{uncor},\text{pri})}$ are the measured values without correction for the first branch, second branch, and the primary vessel, respectively, and d_{sec_1}, d_{sec_2}, and d_{pri} are the diameters of the first branch, second branch, and primary vessel, respectively.

$$k = \frac{SO_{2(\text{uncor},\text{sec}_1)} + SO_{2(\text{uncor},\text{sec}_2)} - 2SO_{2(\text{uncor},\text{pri})}}{2 \cdot d_{\text{pri}} - d_{\text{sec}_1} - d_{\text{sec}_2}} \quad (5)$$

The constant k was then used in Equation 6, where d is the vessel diameter, $\bar{d}$ is the mean vessel diameter, and $SO_{2(\text{cor})}$ is the corrected saturation value.

$$SO_{2(\text{cor})} = k \cdot (d - \bar{d})SO_{2(\text{uncor})} \quad (6)$$

SO_2 values before correction were gathered from the previous section, testing a 92% SO_2 vessel with varying diameter. A theoretical bifurcation based on Murray's principle[61] was assumed, where a primary 120-μm diameter vessel bifurcated into 90-μm and 100-μm diameter branches to calculate the correction factor, k.

Figure 11 displays the corrected SO_2 values for a vessel with a true SO_2 of 92%. The correction works very well when the mean diameter is very close to the diameter of the vessels used to calibrate the algorithms. As shown in Figure 12, if the calibration vessels are larger than the mean diameter, then the correction will shift calculated values of SO_2 up; conversely, if the calibration vessel is smaller than the mean diameter, then the correction will shift the calculated SO_2 values downward. This result greatly reduces the benefit of the compensation.

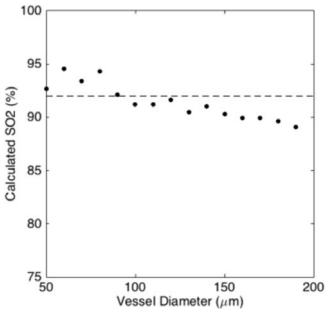

FIGURE 11. Calculated SO_2 after correction for vessel diameter.

Because vessels with 50- to 200-μm diameters are typically analyzed, Figure 12 investigates the results when the two-wavelength algorithms are calibrated with 80, 120, and 180 μm diameter vessels.

Choroidal Crosstalk. In this paper, the choroid has been modeled as a uniform layer containing 70% volume of hemoglobin and 30% volume of melanin similarly to what proposed by Preece and Claridge[55] and Liu et al.[51] Nevertheless, choroidal vessels can often be resolved in long wavelength imagery and disrupt the otherwise homogeneous background of fundus imaging. This section will investigate this phenomenon. For this purpose, we have embedded a small vessel with blood oxygenation of 95% in our standard choroid. The vessel is placed 10 μm below the top of the choroid layer, underneath the test vessel in the retina and parallel to the surface. SO_2 calculations were made on the vessel in the retinal layer. Calculations were performed utilizing the well-calibrated equation, where the SO_2 of both calibration vessels were assumed correctly. Simulations were performed on 96% SO_2, 100-μm test retinal vessels. Choroidal vessel diameters ranged from 20 to 100 μm, with a step size of 10 μm and an SO_2 of 95%. Figure 13b shows the error caused by the introduction of a discrete choroidal vessels in the uniform choroid directly below the vessel in the retina.

Varying Concentration of Melanin in the Choroid. Melanin contributes significantly to the high absorbance of the choroid. It has been demonstrated that this pigmentation has an affect on the accuracy of retinal oximetry.[39,51] Variations in melanin concentration exist among different people, but may also exist in different regions in the eye because the choroid is not a homogenous structure. For these calculations, calibration vessel SO_2 values were assumed correctly. Simulations were performed on 100-μm retinal vessels with 96% SO_2. The concentration of melanin in the choroid was varied from 18 to 40 mg/ml, with a step size of 2 mg/ml.

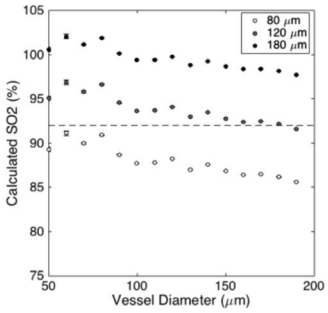

FIGURE 12. Calculated SO_2 after correction for vessel size for measurements calibrated using vessels with diameters of 80 μm, 120 μm, and 180 μm and a mean diameter of 100 μm.

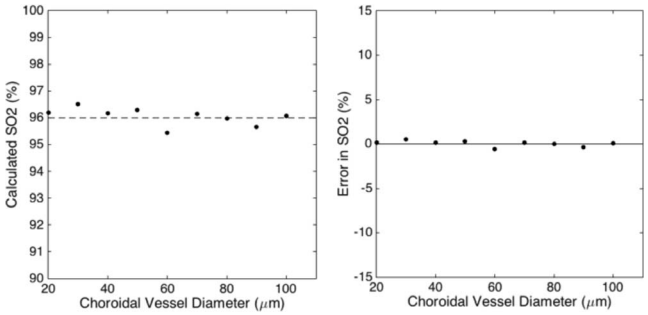

FIGURE 13. (**a**) Calculated SO_2 for varying choroidal vessel diameters. (**b**) Error of the calculated SO_2.

The calibration melanin concentration was kept at 26 mg/ml. As seen in Figure 14, vessel oxygen saturation is overestimated when melanin concentration is higher and is underestimated when melanin concentration is lower. Similar findings were reported by Hammer et al.[39] in their experimental work.

DISCUSSION

We used a three-dimensional, voxel-based Monte Carlo model to investigate the accuracy of two-wavelength algorithms used in novel retinal oximeters. As seen in the results, under ideal circumstances this approach calculates SO_2 values very close to the true value. The most significant errors were found when there were incorrect calibration assumptions, resulting in differences from true values as high as 20 percentage points in SO_2. Recent versions of commercial retinal oximeter do not rely on individual calibration but a set of tabulated data for ODR values of arteries and veins, hence the possibility of large errors in this domain has been reduced.

Vessel size also produced errors, particularly for larger-than-average vessels. The correction method proposed by Geirsdottir et al.[7] worked rather well under ideal circumstances. Some error arises in cases where calibration vessels and test vessels have very different diameters, resulting at times in errors larger than uncorrected SO_2 measurements.

Choroidal crosstalk and choroidal melanin did not show a dramatic production of error, and the correction method used by most investigators was generally successful in improving the measured results. It should be noted that multiple sources of error could occur simultaneously, leading to an accumulation of errors in the calculated oxygenation. Specifically, there may be compounding effects of error from incorrect calibration, vessel size, eye pigmentation, and choroidal crosstalk. Based on our results, the error associated with this technique may be as low as 1 percentage point SO_2 under very ideal circum-

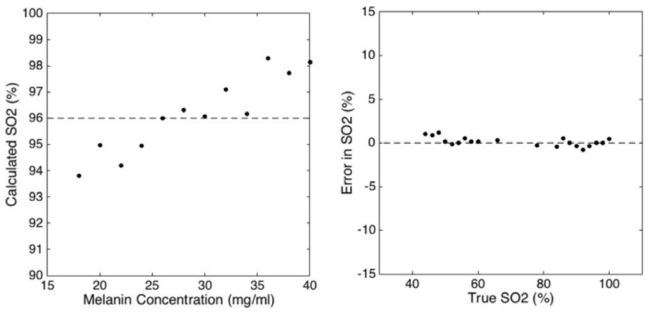

FIGURE 14. (**a**) Calculated SO_2 for different concentrations of melanin in the choroid from 18 to 40 mg/ml. (**b**) Error of calculated SO_2.

stances, but greater than 20 percentage points when a very poor measurement technique is applied.

Other sources of error for retinal oximeters have also been noted by several investigators,[33,62] some pertaining to technical choices for the apparatus. For example, dark current, readout noise, and shot noise camera noise level must be carefully estimated and corrected when using retinal oximeter as they may limit the detector dynamic range and become additive noise in the oximetry measurements. Subtraction of a dark noise images has proven to be essential when acquiring oximetry measurements. Other errors may occur as a result of poor or inconsistent illumination, which would reflect in the calculation of ODR. Here we have limited our study to an ideal scenario of a perfect instrument, but further work needs to be done to characterize the two-wavelength technique in less ideal situations.

Ultimately, as noted by several research groups, retinal oximetry is at a technical stage where good sensitivity and high repeatability can be achieved (avoiding limiting cases such as very small vessels, abnormal choroidal pigmentation, or unusual choroidal hemodynamic). Training of the image reviewer may be necessary to this end. To this date, truly quantitative values of oxygen saturation, although not strictly necessary for longitudinal studies of disease, will require a more robust calibration technique as well as continuous improvement in the reduction of error because of the confounding parameters noted in this paper. Furthermore, the gold standard of retinal oximetry, such as eye phantoms or other noninvasive oximetry techniques, need to be developed to truly test each apparatus.

Acknowledgments

The authors thank Randolph D. Glickman, PhD, and Steve Jacques, PhD, for the valuable discussion about the eye optical properties.

Supported by the Herbert Wertheim College of Medicine and the Herbert and Nicole Wertheim Professorship Endowment.

Disclosure: **D.A. Rodriguez**, None; **T.J. Pfefer**, None; **Q. Wang**, None; **P.F. Lopez**, None; **J.C. Ramella-Roman**, None

References

1. Kohner EM, Patel V, Rassam SM. Role of blood flow and impaired autoregulation in the pathogenesis of diabetic retinopathy. *Diabetes*. 1995;44:603–607.
2. Wangsa-Wirawan ND, Linsenmeier RA. Retinal oxygen: fundamental and clinical aspects. *Arch Ophthalmol*. 2003;121:547–557.
3. Cunningham S, McColm JR, Wade J, Sedowofia K, McIntosh N, Fleck B. A novel model of retinopathy of prematurity simulating preterm oxygen variability in the rat. *Invest Ophthalmol Vis Sci*. 2000;41:4275–4280.
4. Bresnick GH, Mukamel DB, Dickinson JC, Cole DR. A screening approach to the surveillance of patients with diabetes for the presence of vision-threatening retinopathy. *Ophthalmology*. 2000;107:19–24.
5. Abràmoff MD, Reinhardt JM, Russell SR, et al. Automated early detection of diabetic retinopathy. *Ophthalmology*. 2010;117:1147–1154.
6. Hardarson SH, Basit S, Jonsdottir TE, et al. Oxygen saturation in human retinal vessels is higher in dark than in light. *Invest Ophthalmol Vis Sci*. 2009;50:2308–2311.
7. Geirsdottir A, Palsson O, Hardarson SH, et al. Retinal vessel oxygen saturation in healthy individuals. *Invest Ophthalmol Vis Sci*. 2012;53:5433–5442.
8. Olafsdottir OB, Eliasdottir TS, Kristjansdottir JV, Hardarson SH, Stefansson E. Retinal vessel oxygen saturation during 100% oxygen breathing in healthy individuals. *PLoS One*. 2015;10:e0128780.
9. Blondal R, Sturludottir MK, Hardarson SH, Halldorsson GH, Stefánsson E. Reliability of vessel diameter measurements with a retinal oximeter. *Graefes Arch Clin Exp Ophthalmol*. 2011;249:1311–1317.
10. Palsson O, Geirsdottir A, Hardarson SH, Olafsdottir OB, Kristjansdottir JV, Stefánsson E. Retinal oximetry images must be standardized: a methodological analysis. *Invest Ophthalmol Vis Sci*. 2012;53:1729–1733.
11. Hardarson SH, Stefánsson E. Retinal oxygen saturation is altered in diabetic retinopathy. *Br J Ophthalmol*. 2012;96:560–563.
12. Jorgensen CM, Hardarson SH, Bek T. The oxygen saturation in retinal vessels from diabetic patients depends on the severity and type of vision-threatening retinopathy. *Acta Ophthalmol*. 2014;92:34–39.
13. Traustason S, Hardarson SH, Gottfredsdottir MS, et al. Dorzolamide-timolol combination and retinal vessel oxygen saturation in patients with glaucoma or ocular hypertension. *Br J Ophthalmol*. 2009;93:1064–1067.
14. Hardarson SH, Gottfredsdottir MS, Halldorsson GH, et al. Glaucoma filtration surgery and retinal oxygen saturation. *Invest Ophthalmol Vis Sci*. 2009;50:5247–5250.
15. Olafsdottir OB, Hardarson SH, Gottfredsdottir MS, Harris A, Stefánsson E. Retinal oximetry in primary open-angle glaucoma. *Invest Ophthalmol Vis Sci*. 2011;52:6409–6413.
16. Vandewalle E, Abegão Pinto L, Olafsdottir OB, et al. Oximetry in glaucoma: correlation of metabolic change with structural and functional damage. *Acta Ophthalmol*. 2014;92:105–110.
17. Olafsdottir OB, Vandewalle E, Abegão Pinto L, et al. Retinal oxygen metabolism in healthy subjects and glaucoma patients. *Br J Ophthalmol*. 2014;98:329–333.
18. Traustason S, Jensen AS, Arvidsson HS, Munch IC, Søndergaard L, Larsen M. Retinal oxygen saturation in patients with systemic hypoxemia. *Invest Ophthalmol Vis Sci*. 2011;52:5064–5067.
19. Geirsdottir A, Hardarson SH, Olafsdottir OB, Stefánsson E. Retinal oxygen metabolism in exudative age-related macular degeneration. *Acta Ophthalmol*. 2014;92:27–33.
20. Eysteinsson T, Hardarson SH, Bragason D, Stefánsson E. Retinal vessel oxygen saturation and vessel diameter in retinitis pigmentosa. *Acta Ophthalmol*. 2014;92:449–453.
21. Hardarson SH, Stefansson E. Oxygen saturation in central retinal vein occlusion. *Am J Ophthalmol*. 2010;150:871–875.
22. Hardarson SH, Stefansson E. Oxygen saturation in branch retinal vein occlusion. *Acta Ophthalmol*. 2012;90:466–470.
23. Eliasdottir TS, Bragason D, Hardarson SH, Kristjansdottir G, Stefánsson E. Venous oxygen saturation is reduced and variable in central retinal vein occlusion. *Graefes Arch Clin Exp Ophthalmol*. 2015;253:1653–1661.
24. Hardarson SH, Elfarsson A, Agnarsson BA, Stefánsson E. Retinal oximetry in central retinal artery occlusion. *Acta Ophthalmol*. 2013;91:189–190.
25. Man RE, Kawasaki R, Wu Z, et al. Reliability and reproducibility of retinal oxygen saturation measurements using a predefined peri-papillary annulus. *Acta Ophthalmol*. 2013;91:e590–e594.
26. Turksever C, Orgul S, Todorova MG. Reproducibility of retinal oximetry measurements in healthy and diseased retinas. *Acta Ophthalmol*. 2015;93:e439–e445.
27. Beach J. Pathway to retinal oximetry. *Trans Vis Sci Tech*. 2014;3:2.
28. Hickam JB, Frayser R, Ross JC. A study of retinal venous blood oxygen saturation in human subjects by photographic means. *Circulation*. 1963;27:375–385.
29. Beach JM, Schwenzer KJ, Srinivas S, Kim D, Tiedeman JS. Oximetry of retinal vessels by dual-wavelength imaging:

calibration and influence of pigmentation. *J Appl Physiol*. 1999;86:748–758.

30. Hardarson SH. Retinal oximetry. *Acta Ophthalmol*. 2013;91: 489–490.
31. Pittman RN, Duling BR. A new method for the measurement of percent oxyhemoglobin. *J Appl Physiol*. 1975;38:315–320.
32. Delori FC. Noninvasive technique for oximetry of blood in retinal vessels. *Appl Opt*. 1988;27:1113–1125.
33. Smith MH. Optimum wavelength combinations for retinal vessel oximetry. *Appl Opt*. 1999;38:258–267.
34. Kashani AH, Kirkman E, Martin G, Humayun MS. Hyperspectral computed tomographic imaging spectroscopy of vascular oxygen gradients in the rabbit retina in vivo. *PLoS One*. 2011;6:e24482.
35. Shahidi AM, Patel SR, Flanagan JG, Hudson C. Regional variation in human retinal vessel oxygen saturation. *Exp Eye Res*. 2013;113:143–147.
36. Mordant DJ, Al-Abboud I, Muyo G, Gorman A, Harvey AR, McNaught AI. Oxygen saturation measurements of the retinal vasculature in treated asymmetrical primary open-angle glaucoma using hyperspectral imaging. *Eye (Lond)*. 2014;28: 1190–1200.
37. Boeckaert J, Vandewalle E, Stalmans I. Oximetry: recent insights into retinal vasopathies and glaucoma. *Bull Soc Belge Ophtalmol*. 2012;319:75–83.
38. Hammer M, Vilser W, Riemer T, et al. Diabetic patients with retinopathy show increased retinal venous oxygen saturation. *Graefes Arch Clin Exp Ophthalmol*. 2009;247:1025–1030.
39. Hammer M, Vilser W, Riemer T, Schweitzer D. Retinal vessel oximetry-calibration, compensation for vessel diameter and fundus pigmentation and reproducibility. *J Biomed Opt*. 2008; 13:054015.
40. Hardarson SH, Harris A, Karlsson RA, et al. Automatic retinal oximetry. *Invest Ophthalmol Vis Sci*. 2006;47:5011–5016.
41. Buerk DG, Shonat RD, Riva CE, Cranstoun SD. O2 gradients and countercurrent exchange in the cat vitreous humor near retinal arterioles and venules. *Microvasc Res*. 1993;45:134–148.
42. Harris A, Dinn RB, Kagemann L, Rechtman E. A review of methods for human retinal oximetry. *Ophthalmic Surg Lasers Imaging*. 2003;34:152–164.
43. Heitmar R, Kalitzeos AA. Reliability of retinal vessel calibre measurements using a retinal oximeter. *BMC Ophthalmol*. 2015;15:184.
44. Smith MH, Denninghoff KR, Lompado A, Hillman LW. Effect of multiple light paths on retinal vessel oximetry. *Appl Opt*. 2000; 39:1183–1193.
45. Pfefer TJ, Kehlet Barton J, Chan EK, et al. A three-dimensional modular adaptable grid numerical model for light propagation during laser irradiation of skin tissue. *IEEE J Sel Top Quant*. 1996;2:934–942.
46. Le du VN, Wang Q, Ramella-Roman JC, Pfefer TJ. Monte Carlo modeling of light-tissue interactions in narrow band imaging. *J Biomed Opt*. 2013;18:10504.
47. Schweitzer D, Hammer M, Kraft J, Thamm E, Königsdörffer E, Strobel J. In vivo measurement of the oxygen saturation of retinal vessels in healthy volunteers. *IEEE Trans Biomed Eng*. 1999;46:1454–1465.
48. de Kock JP, Tarassenko L, Glynn CJ, Hill AR. Reflectance pulse oximetry measurements from the retinal fundus. *IEEE Trans Biomed Eng*. 1993;40:817–823.
49. Bosschaart N, Edelman GJ, Aalders MC, van Leeuwen TG, Faber DJ. A literature review and novel theoretical approach on the optical properties of whole blood. *Lasers Med Sci*. 2014;29:453–479.
50. Wang L, Jacques SL, Zheng L. MCML–Monte Carlo modeling of light transport in multi-layered tissues. *Comput Methods Programs Biomed*. 1995;47:131–146.
51. Liu W, Jiao S, Zhang HF. Accuracy of retinal oximetry: a Monte Carlo investigation. *J Biomed Opt*. 2013;18:066003.
52. Hammer M, Roggan A, Schweitzer D, Müller G. Optical-properties of ocular fundus tissues—an in-vitro study using the double-integrating-sphere technique and inverse Monte-Carlo simulation. *Phys Med Biol*. 1995;40:963–978.
53. Glickman RD, Jacques SL, Hall RM, Kumar N. Revisiting the internal absorption coefficient of the retinal pigment epithelium melanosome. *Proc SPIE Int Soc Opt Eng*. 2001;4257:134–141.
54. Feeney-Burns L, Hilderbrand ES, Eldridge S. Aging human RPE: morphometric analysis of macular, equatorial, and peripheral cells. *Invest Ophthalmol Vis Sci*. 1984;25:195–200.
55. Preece SJ, Claridge E. Monte Carlo modelling of the spectral reflectance of the human eye. *Phys Med Biol*. 2002;47:2863–2877.
56. Hammer M, Schweitzer D, Thamm E, Kolb A. Non-invasive measurement of the concentration of melanin, xanthophyll and hemoglobin in single fundus layers in vivo by fundus reflectometry. *Int Ophthalmol*. 2001;23(4–6):279–289.
57. Koblova EV, Bashkatov AN, Genina EA, Tuchin VV, Bakutkin VV. Estimation of melanin content in iris of human eye. *Proc SPIE Int Soc Opt Eng*. 2005;5688:302–311.
58. Henyey LG, Greenstein JL. Diffuse radiation in the galaxy. *Astrophys J*. 1941;93:70–83.
59. Hammer M, Yaroslavsky AN, Schweitzer D. A scattering phase function for blood with physiological haematocrit. *Phys Med Biol*. 2001;46:N65–N69.
60. Ibrahim MA, Annam RE, Sepah YJ, et al. Assessment of oxygen saturation in retinal vessels of normal subjects and diabetic patients with and without retinopathy using Flow Oximetry System. *Quant Imaging Med Surg*. 2015;5:86–96.
61. Murray CD. The physiological principle of minimum work applied to the angle of branching of arteries. *J Gen Physiol*. 1926;9:835–841.
62. Mordant DJ, Al-Abboud I, Muyo G, et al. Validation of human whole blood oximetry, using a hyperspectral fundus camera with a model eye. *Invest Ophthalmol Vis Sci*. 2011;52:2851–2859.

Investigative Ophthalmology & Visual Science